

Multicompartment Micelles from ABC Miktoarm Stars in Water

Zhibo Li,¹ Ellina Kesselman,³ Yeshayahu Talmon,³
Marc A. Hillmyer,^{1*} Timothy P. Lodge^{1,2*}

By combining three mutually immiscible polymeric components in a mixed-arm star block terpolymer architecture, we have observed the formation of a previously unknown class of multicompartment micelles in dilute aqueous solution. Connection of water-soluble poly(ethylene oxide) and two hydrophobic but immiscible components (a polymeric hydrocarbon and a perfluorinated polyether) at a common junction leads to molecular frustration when dispersed in aqueous solution. The incompatible hydrophobic blocks form cores that are protected from the water by the poly(ethylene oxide) blocks, but both are forced to make contact with the poly(ethylene oxide) by virtue of the chain architecture. The structures that emerge depend on the relative lengths of the blocks and can be tuned from discrete multicompartment micelles to extended wormlike structures with segmented cores.

The spontaneous self-assembly of amphiphilic molecules into discrete supramolecular assemblies and two- and three-dimensional macrolattices has been used in the development of many new nanotechnological applications, including nanolithography (1), biomineralization (2), and drug delivery (3). Indeed, such free energy-driven processes have been touted as the exemplar of bottom-up engineering (4). Block copolymers, which consist of macromolecules formed by covalent end-linking of two or more disparate polymeric blocks, represent a particularly appealing template material. They potentially combine traditional attributes of polymeric materials with sophisticated functions (e.g., luminescence, conductivity, and storage and release of active molecules) (5–7). As a design platform, they offer a host of control variables through which structure may be tuned, including block length, polymer architecture, choice of monomers, and selection of interaction strengths. The ability of two-monomer diblock (AB) copolymers to form micelles is well documented (5, 8, 9). As with their lower-molar-mass surfactant and lipid analogs, the predominant micellar morphologies formed are spheres, cylinders, and vesicles, the last corresponding to nearly flat bilayer sheets curved around to form a sealed container.

The structures available with AB copolymers are all limited to partitioning of space into an “inside” and an “outside.” In contrast, the possibilities inherent in multi-

compartment micellar structures have recently been recognized (10). A biological analogy is apt: Prokaryotic systems such as bacteria have a single lipid bilayer dividing space and thus are analogous to vesicular assemblies in AB copolymers, whereas eukaryotic cells, with multiple functional units (nucleus, organelles, etc.) contained within one overall membrane, are the paradigm for a multicompartment system (11). For example, copolymer micelles and vesicles are being extensively investigated for drug delivery applications (3, 12). A multicompartment system could deliver simultaneously two or more active but incompatible agents in precise stoichiometric proportions. Some progress toward multicompartment micelles has been reported (13–15); examples using linear ABC triblocks include core-shell-corona spheres (16) and disks (17). In these cases, the subdivision of the micellar interior is limited to two concentric nanodomains.

There are several design criteria to consider in developing suitable ABC terpolymers. Clearly one key feature is a strong effective repulsion between each pair of blocks, such that A, B, and C segregate into distinct nanodomains. The segregation strength in polymers is quantified by the dimensionless product χN , where χ is the monomer-monomer interaction parameter and N is the degree of polymerization (18). However, limited solubility, kinetics of structural equilibration, and synthetic convenience all favor relatively modest molecular weights (small N), requiring that the three pairwise χ parameters be very large. The chosen monomers must also be amenable to controlled polymerization schemes in order to prepare blocks of well-defined length. To this end, we selected a water-soluble poly(ethylene oxide) (O) block, a saturated hydrocarbon

polyethylethylene (E) block, and a hydrophobic, lipophobic poly(perfluoropropylene oxide) (F) block. The hydrophilic O block has the largest N , to enhance water solubility. The final design feature is the chain architecture; for example, ABC, ACB, and BAC triblocks can adopt quite different bulk morphologies, even if the block lengths remain constant, due to the competition between “desirable” interfaces (those between the blocks with the smallest χ) and “mandatory” interfaces (those between covalently linked blocks) (19–21). With this in mind, we have targeted miktoarm star ABC terpolymers (Fig. 1) (22), whereby the three-fold connector enforces a one-dimensional locus of terpolymer junctions along which the three nanodomains must intersect (23). This strategy in particular suppresses formation of core-shell-corona structures in favor of multicompartment micelles. Furthermore, this architecture combines the rather short E and F blocks to impose appealingly small (<10 nm) elementary compartments.

The structure of the ABC miktoarm star block terpolymers is given in Fig. 1. The details of the synthetic protocol will be presented elsewhere (24). Briefly, butadiene is polymerized anionically and terminated with a heterobifunctional protected initiator. The resulting hydroxyl end-functionalized polybutadiene is hydrogenated to polyethylene. This end-functionalized E block serves as a macroinitiator for anionic polymerization of ethylene oxide, yielding the O block. After capping the O block with ethylbromide and deprotection of a hydroxyl group located at the juncture of the E and O blocks, acid chloride end-functionalized F blocks are coupled with this hydroxyl group. The resulting miktoarm stars are designated μ -EOF(x - y - z), where x , y , and z represent the E, O, and F block molecular weights, respectively, in kD (table S1). This overall protocol is conveniently modular, in that a given batch of E may be used to prepare a series of EO diblocks of varying O content,

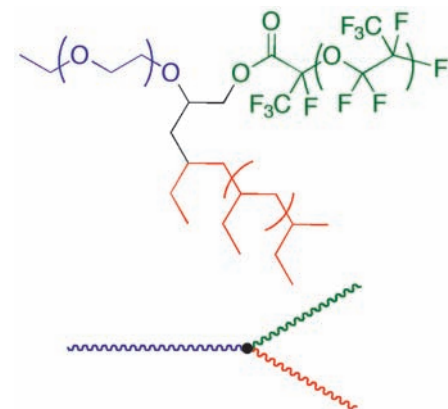


Fig. 1. Chemical structure and schematic representation of μ -EOF star block terpolymers.

¹Department of Chemistry, ²Department of Chemical Engineering and Materials Science, University of Minnesota, Minneapolis, MN 55455, USA. ³Department of Chemical Engineering, Technion-Israel Institute of Technology, Haifa 32000, Israel.

*To whom correspondence should be addressed. E-mail: lodge@chem.umn.edu (T.P.L.); hillmyer@chem.umn.edu (M.A.H.)

and these diblocks in turn may be conjugated to a series of F blocks. A series of μ -EOF polymers were prepared, and in all cases the molecular weight distributions were narrow (polydispersity indices range from 1.1 to 1.3).

We have used a variety of experimental techniques to characterize micellar structures formed in dilute aqueous solutions (25), but, in situations where rather complicated, irregular, and polydisperse aggregates are anticipated, direct imaging by cryo-transmission electron microscopy (cryo-TEM) is the method of choice. Samples are prepared by suspending 100- to 200-nm-thick menisci of 1 weight percent aqueous solutions on a lacy carbon film, which is then rapidly immersed in liquid ethane at its freezing point. The resulting vitreous water preserves the possibly delicate self-assembled structures, which are then imaged without staining, in transmission, at about -175°C , by using very low electron exposures. Further details of the cryo-TEM technique may be found elsewhere (26, 27).

Typical cryo-TEM images from 1 wt % solutions of μ -EOF(2-13-2) and μ -EOF(2-13-3) are shown in Fig. 2, A to D (also figs. S1 and S2). Figure 2A reveals a preponderance of distinct micellar cores with sizes of about 12 ± 2 nm, each of which contains irregular

small dark regions (28). The dark regions (highest electron density) are attributable to the F nanodomains because they minimize contact with the surrounding aqueous phase, with the remainder of the core (gray regions) made up of the E blocks. The O coronas are not directly visible because they are well solvated, but their presence and spatial extent is indicated by the typical separation distances between neighboring cores. The apparent order in the micrographs is the result of specimen preparation. In some instances, the F domains are larger and more distinct (Fig. 2, B to D). Here, fascinating three-lobe and four-lobe micellar cores can be discerned, with the lighter gray E domains more spherical and the darker F domains filling the interstitial spaces.

The results in Fig. 2 reflect the stars with the largest hydrophilic (O) block. Images for stars with shorter O blocks are shown in Fig. 3, A to D. In these cases, elongated, wormlike structures are obtained, and furthermore the worms are layered or segmented along the long axis. Specifically, in Fig. 3A (also fig. S3) μ -EOF(2-7-2) exhibits long "strings" of dark cores in addition to discrete micelles. These results imply an attractive interaction between micelles, which is initially surprising given the steric repulsion arising from the O corona. In addition,

the attraction is apparently uniaxial, leading exclusively to strings of micelles. We propose that the individual micellar elements contain an oblate disk-like F core, surrounded top and bottom by an E shell (Fig. 4A). Because the O blocks must emanate from the E-F interface and curl around the top and bottom of the micelle to screen the hydrophobic core, a natural explanation for the uniaxial attraction emerges. As two micelles approach one another, any fluctuation in O concentration in the corona can expose the hydrophobic core components. In forming a string, the different cores are able to share their O coronas, thus protecting them from the highly unfavorable exposure to water.

"Segmented worm" micelles formed by μ -EOF(2-9-2), μ -EOF(2-9-3), and μ -EOF(2-9-5) are shown in Fig. 3, B to D, respectively (also figs. S4 to S6). In this series of molecules with increasing F block compositions, a variety of overall micellar shapes and sizes are evident, and a consistent local packing motif persists, namely alternating flat disks of dark (F) and gray (E), each about 5 to 7 nm in thickness. As in the previous case, the O coronas are shared, forming cylindrical structures; the difference from Fig. 3A lies in the flatness of the E and F domains. The proposed chain packing in the segmented worms is illustrated in Fig. 4B. The O coronas are anchored around circles formed at the intersection of each E and F disk. Within the disks, the E and F chains are almost fully extended. For example, the apparent radii of the segmented worms are about 6 to 7 nm, 7 to 8 nm, and 9 to 10 nm in the μ -EOF(2-9-2), μ -EOF(2-9-3), and μ -EOF(2-9-5) samples, respectively. The fully extended F block in each case would be about 5, 7.5, and 11.5 nm, respectively, consistent with the proposed chain packing motif in Fig. 4B. The fully extended E block would be about 8 nm in all cases. The thickness of each segment combined with the known densities of E and F indicates an aggregation number of 350 to 450 for each repeat unit of the segmented worm.

Although a rich variety of multicompartiment micellar structures are revealed in Figs. 2 and 3, they can be understood at least qualitatively through the interplay of a few factors. First, the three components (E, F, and O plus water) are strongly incompatible, leading to the formation of distinct domains. In fact, this system probably lies in the so-called superstrong segregation regime (SSSR) (29, 30), in which the interfacial energies overwhelm the entropic penalties for stretching the shorter blocks. One consequence of the SSSR is that flat interfaces are preferred. Also, the E and F domain sizes are limited by chain length; they cannot stretch beyond the fully extended block size. Second, although the extremely large interfacial ten-

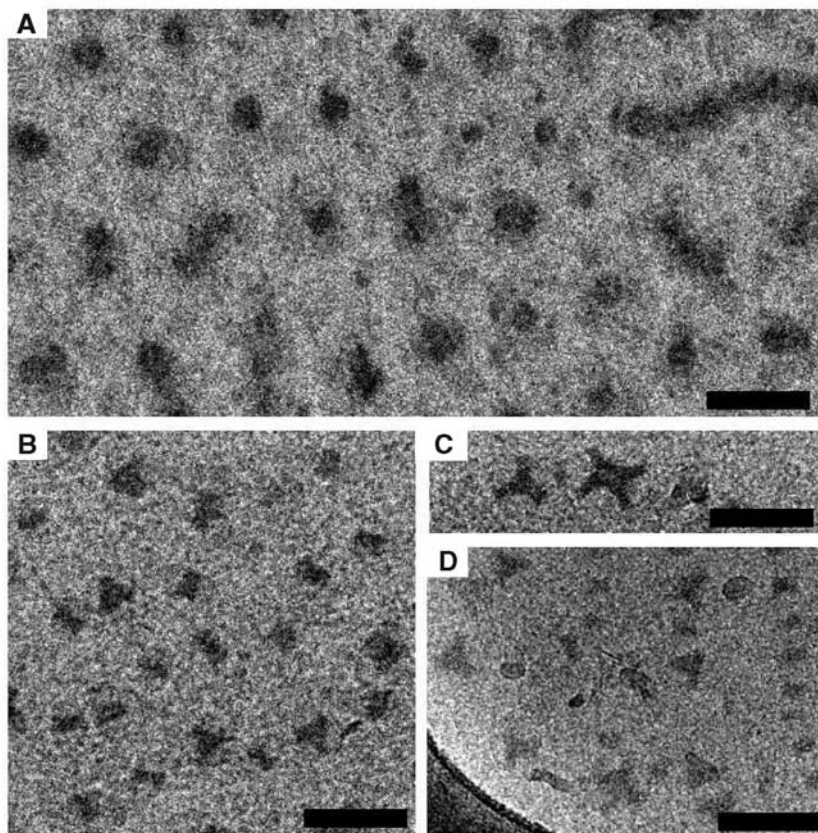


Fig. 2. Cryo-TEM images of 1 wt % aqueous solutions of μ -EOF(2-13-2) (A) and μ -EOF(2-13-3) (B to D); scale bars indicate 50 nm.

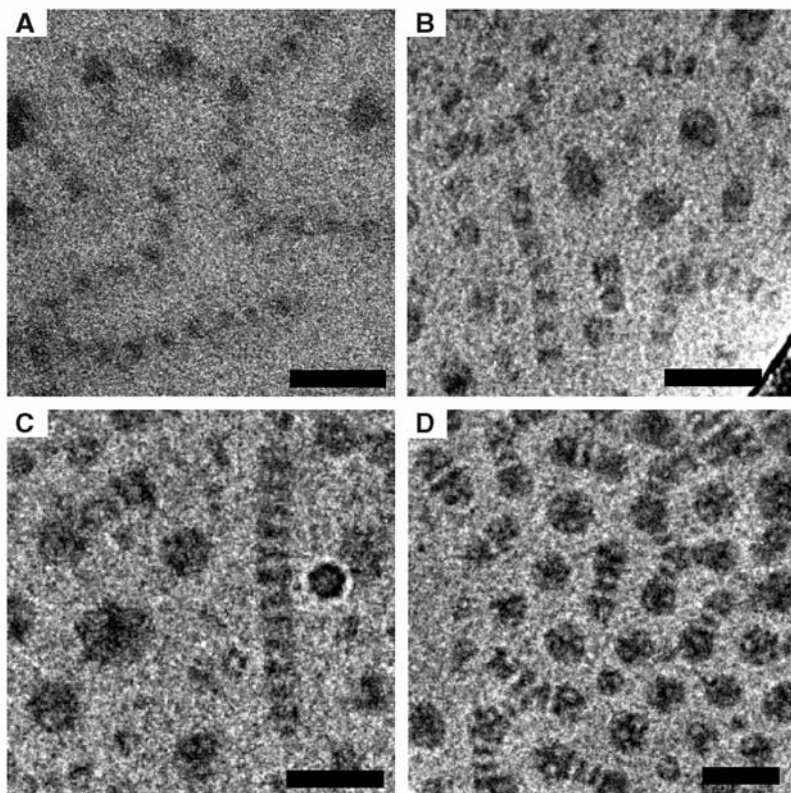


Fig. 3. Cryo-TEM images of 1 wt % aqueous solutions of (A) μ -EOF(2-7-2), (B) μ -EOF(2-9-2), (C) μ -EOF(2-9-3), and (D) μ -EOF(2-9-5); scale bars indicate 50 nm.

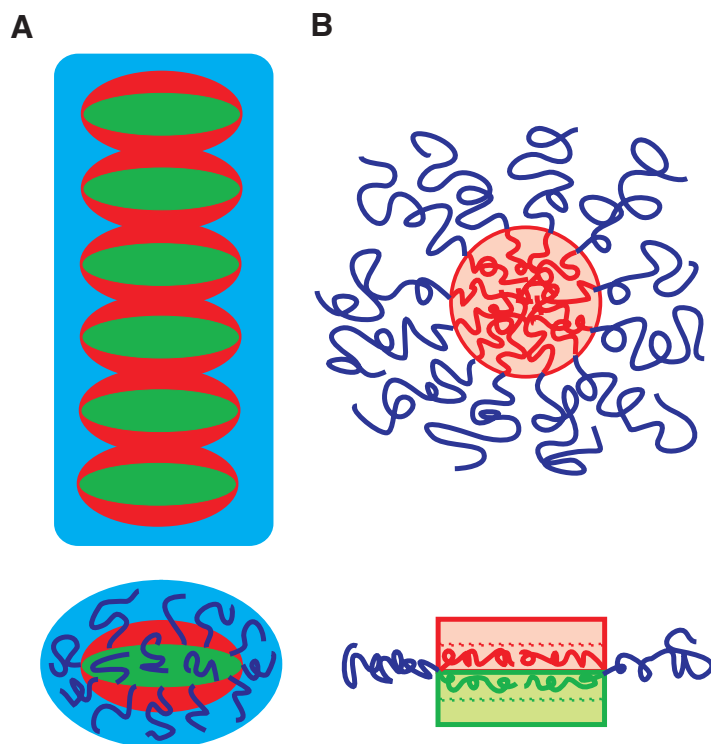


Fig. 4. Schematic drawing of (A) an individual μ -EOF(2-7-2) micelle and the stacking into a string as in Fig. 3A; (B) side and end-on views of proposed chain packing for μ -EOF segmented worms in Fig. 3, B to D.

sions favor flat interfaces, this comes into conflict with the terpolymer composition, in which the longer and well-solvated O blocks favor high interfacial curvature. Because the O-F interfacial tension should be even greater than the (still large) O-E and E-F interfacial tensions, the chains pack as best they can to shield F from O. However, by virtue of the covalent connectivity of F and O in the star architecture (Fig. 1), some contact between F and O is inevitable. This, in turn, imposes constraints on the dimensions of the core compartments. Lastly, for each terpolymer a distribution of micellar aggregates is observed. This is indicative of a nonergodic system, as has already been documented in aqueous diblocks (31); the system is unable to find the global free energy minimum, because the exchange of chains between micelles is prohibitively slow. Nevertheless, the various local minima share a small number of common packing motifs, because chains within a given aggregate are able to adjust their packing and conformation.

With these considerations in mind, the discrete micelles favored by μ -EOF(2-13-2) and μ -EOF(2-13-3) (Fig. 2) can be attributed to the longest O blocks dictating a high interfacial curvature. Within each core, the F blocks segregate into one or more domains; the smaller the domain, the greater the opportunity for the anchors of the O blocks to be dispersed uniformly across the surfaces of the core. Nevertheless, these terpolymers also form the three- and four-lobe cores illustrated in Fig. 2, B to D; here, the E-F interfaces are flatter, and the F blocks are generally shielded from O by the E domains. Similarly, the segmented worms that are observed for the terpolymers with shorter O blocks have flatter O-F and O-E interfaces, indicating the smaller role of corona crowding. The segmented worm and micellar strings shown in Fig. 3, A to D, are all formed by terpolymers with shorter O blocks. The immediate consequence of this is the prevalence of extended structures, whereby the core surface area per O chain is reduced and the E-F interfaces are flatter. The numerical considerations given above also confirm that the individual hydrophobic blocks adopt nearly fully extended conformations, consistent with the SSSR.

These results demonstrate a strategy for forming multicompartiment micelles. Although there is a large parameter space to explore (e.g., block lengths, choice of monomers, and chain architecture), these results already give indications of the relative block lengths needed to favor discrete, multidomain cores [i.e., μ -EOF(2-13-2) and μ -EOF(2-13-3)] or extended, segmented worm structures. The choice of fluorocarbon and hydrocarbon blocks allows access to the SSSR, even for relatively modest molecular weights, and the miktoarm star architecture is remarkably

successful in promoting formation of multi-compartment cores (32).

References and Notes

- M. Park, C. Harrison, P. M. Chaikin, R. A. Register, D. H. Adamson, *Science* **276**, 1401 (1997).
- J. H. Collier, P. B. Messersmith, *Annu. Rev. Mater. Res.* **31**, 237 (2001).
- R. Savić, L. Luo, A. Eisenberg, D. Maysinger, *Science* **300**, 615 (2003).
- M. Shimomura, T. Sawadaishi, *Curr. Opin. Colloids Interface Sci.* **6**, 11 (2001).
- I. W. Hamley, *The Physics of Block Copolymers* (Oxford Univ. Press, New York, 1998).
- C. Park, J. Yoon, E. L. Thomas, *Polymer* **44**, 6725 (2003).
- T. P. Lodge, *Macromol. Chem. Phys.* **204**, 265 (2003).
- G. Riess, *Prog. Polymer Sci.* **28**, 1107 (2003).
- A. Halperin, M. Tirrell, T. P. Lodge, *Adv. Polym. Sci.* **100**, 31 (1991).
- A. Laschewsky, *Curr. Opin. Colloids Interface Sci.* **8**, 274 (2003).
- E. T. Kisak, B. Coldren, C. A. Evans, C. Boyer, J. A. Zasadzinski, *Curr. Med. Chem.* **11**, 199 (2004).
- D. E. Discher, A. Eisenberg, *Science* **297**, 967 (2002).
- A. Kotzev, A. Laschewsky, P. Adriaensens, J. Gelan, *Macromolecules* **35**, 1091 (2002).
- K. Stähler, J. Selb, F. Candau, *Langmuir* **15**, 7565 (1999).
- R. Weberskirch, J. Preuschen, H. W. Spiess, O. Nuyken, *Macromol. Chem. Phys.* **201**, 995 (2000).
- J.-F. Gohy, N. Willet, S. Varshney, J.-X. Zhang, R. Jérôme, *Angew. Chem. Int. Ed. Engl.* **40**, 3214 (2001).
- Z. Zhou, Z. Li, Y. Ren, M. A. Hillmyer, T. P. Lodge, *J. Am. Chem. Soc.* **125**, 10182 (2003).
- F. S. Bates, *Science* **251**, 898 (1991).
- A. Balsamo et al., *Macromolecules* **36**, 4515 (2003).
- T. S. Bailey, C. M. Hardy, T. H. Epps, F. S. Bates, *Macromolecules* **35**, 7007 (2002).
- T. Goldacker, V. Abetz, R. Stadler, I. Erukhimovich, L. Leibler, *Nature* **398**, 137 (1999).
- N. Hadjichristidis, *J. Polym. Sci. Polym. Chem.* **37**, 857 (1999).
- S. Sioula, N. Hadjichristidis, E. L. Thomas, *Macromolecules* **31**, 8429 (1998).
- Z. Li, M. A. Hillmyer, T. P. Lodge, unpublished results.
- Dynamic light scattering (DLS) data on dilute aqueous solutions of the μ -EOF samples were consistent with the cryo-TEM images. Namely, we typically observed a rather narrow distribution of relatively small micelles with hydrodynamic radii, in agreement with discrete micellar-like aggregates (Fig. 2), as well as a population of larger hydrodynamic particles consistent with the strings shown in Fig. 3. A description of the DLS technique and representative data (fig. S7) are given in (26).
- Details of the cryo-TEM measurements and representative images of μ -EOF solutions with large fields of view are given on Science Online.
- D. Danino, A. Bernheim-Groswasser, Y. Talmon, *Colloid Surf. A Physicochem. Eng.* **183**, 113 (2001).
- E. E. Dormidontova, A. R. Khokhlov, *Macromolecules* **30**, 1890 (1997).
- A. N. Semenov, I. A. Nyrkova, A. R. Khokhlov, *Macromolecules* **28**, 7491 (1995).
- T. P. Lodge, M. A. Hillmyer, Z. Zhou, Y. Talmon, *Macromolecules* **37**, 6680 (2004).
- S. Jain, F. S. Bates, *Science* **300**, 460 (2003).
- This work was supported primarily by the Materials Research Science and Engineering Center program of NSF under award no. DMR-0212302.

Supporting Online Material

www.sciencemag.org/cgi/content/full/306/5693/98/DC1

Materials and Methods

Figs. S1 to S7

Table S1

References

28 July 2004; accepted 20 August 2004

Cope's Rule, Hypercarnivory, and Extinction in North American Canids

Blaire Van Valkenburgh,^{1*} Xiaoming Wang,² John Damuth³

Over the past 50 million years, successive clades of large carnivorous mammals diversified and then declined to extinction. In most instances, the cause of the decline remains a puzzle. Here we argue that energetic constraints and pervasive selection for larger size (Cope's rule) in carnivores lead to dietary specialization (hypercarnivory) and increased vulnerability to extinction. In two major clades of extinct North American canids, the evolution of large size was associated with a dietary shift to hypercarnivory and a decline in species durations. Thus, selection for attributes that promoted individual success resulted in progressive evolutionary failure of their clades.

The history of large (>7 kg) predatory mammals is one of repeated ecological replacement (1). The various ecomorphological roles of cat-like, wolf-like, and hyena-like predator have been filled by representatives of distinct families at different times. In general, a single subfamily or family diversified and dominated a given ecomorphological role for about 10 million years and then declined, only to be replaced by a new clade. The expansion phase is often explained as a result of key adaptations and/or ecological opportunity, but it has been

more difficult to understand the decline to extinction of a formerly successful group. Here we use the recently documented and exceptionally rich fossil record of North American canids (2, 3) as a test case for studying the dynamics of extinction.

The dog family Canidae has three subfamilies: the extant Caninae, the extinct Hesperocyoninae [40 to 15 million years ago (Ma)], and the Borophaginae (34 to 2 Ma) (4). Both extinct subfamilies were endemic to North America and were very diverse in the Miocene, reaching a peak of 25 contemporaneous species approximately 30 Ma (Fig. 1A). The fossil record of these canids is impressive and well studied, with at least 28 species of hesperocyoninines and 68 species of borophaginae described (2, 3, 5). In dental specialization and inferred diets, hesperocyoninines ranged from relatively unspecialized mesocarnivores (inferred diet of small prey and plant matter) to more specialized hypercarni-

vores (inferred diet of large prey) characterized by enhanced shearing blades on their molar teeth (2). The more diverse borophaginae included both of these types, as well as hypocarnivores (inferred diet of more plant matter than mesocarnivores) with reduced shearing blades and enlarged grinding areas on their molars (3).

To examine trends in body size and dietary specialization in fossil canids, we relied on inferences from dental morphology. Based on the established correlation between lower carnassial tooth [first molar (M_1)] length and body mass in living canids, we used M_1 length as a surrogate for body mass (6, 7). To estimate dietary adaptations, we relied on previous studies of the correspondence between morphology and diet in canids (8, 9). A discriminant analysis of 30 craniodental measurements on 27 species of modern canids easily separated hypercarnivores as having relatively deep jaws, large canine and incisor teeth, reduced molar grinding areas, and longer shearing blades on their lower carnassials (9). Because fossil species are rarely represented by complete specimens, we focused on three shape indices (six measurements) that together are highly informative about canid diets, independent of body mass. These are jaw depth relative to length, the proportion of the lower carnassial devoted to shearing rather than grinding function, and the proportion of the upper carnassial and molars devoted to grinding rather than shearing (10). Relative to hypo- and mesocarnivores, hypercarnivores tend to have deeper jaws to withstand loads imposed by killing and feeding on large prey, as well as long shearing blades and reduced molar grinding areas.

In both subfamilies, mean body mass increased substantially with time (Fig. 1, B and C) and within-lineage transitions to larger size significantly exceeded those to smaller

¹Department of Ecology and Evolutionary Biology, University of California at Los Angeles, Los Angeles, CA 90095-1606, USA. ²Department of Vertebrate Paleontology, Natural History Museum of Los Angeles County, 900 Exposition Boulevard, Los Angeles, CA 90007, USA. ³Department of Ecology, Evolution, and Marine Biology, University of California at Santa Barbara, Santa Barbara, CA 93106, USA.

*To whom correspondence should be addressed. E-mail: bvanval@ucla.edu